

## Discovery of New Inhibitors of Enoyl-ACP Reductase *via* Structure-Based Virtual Screening

A. Laoud<sup>a,b,\*</sup>, F. Ali-Rachedi<sup>c</sup> and F. Ferkous<sup>a</sup>

<sup>a</sup>LCOA: Laboratoire de Chimie Organique Appliquée, Département de Chimie, Faculté des Sciences, Université Badji-Mokhtar-Annaba, BP 12, Annaba, Algérie

<sup>b</sup>Département de Science de la Matière, Faculté de Science de la Matière, Université Ibn Khaldoun-Tiaret, Algérie

<sup>c</sup>Faculté des Science et la Technologie, Université Souk Ahras, PB 1553, 41000 Souk Ahras, Algérie

(Received 18 May 2022, Accepted 18 July 2022)

A virtual screening protocol combining a 3D-QSAR model with molecular docking procedures and physicochemical properties was used to find novel inhibitors of enoyl-acyl carrier protein (ACP) reductase against *Mycobacterium tuberculosis*. Initially, 32 isoniazid analogues were collected from literature and investigated against the tuberculosis target (PDB Id: 2IE0) using molecular docking. The docking studies were used to position the inhibitors into the active site of enoyl-ACP reductase to derive a receptor-based 3D-QSAR model. The 3D-QSAR model was built and shown to be statistically significant, with a high predictive ability for the training ( $R^2 = 0.97$ ) and test ( $Q^2 = 0.73$ ) sets. The analysis of the contour cubes derived from the 3D-QSAR model revealed the chemical features necessary for the inhibition of the enoyl-ACP reductase enzyme. The model was then used for virtual screening with the aim of identifying new inhibitors of enoyl-ACP reductase and predicting their potential activity. Based on the results of the above studies, 10 new molecules were proposed as enoyl-ACP reductase inhibitors with high binding affinity, activity prediction, and favorable ADME properties.

**Keywords:** 3D-QSAR, Tuberculosis, Virtual screening, ADME, Molecular docking

## INTRODUCTION

Tuberculosis (TB) is an infectious bacterial disease caused by *Mycobacterium tuberculosis* (Mtb) and is one of the top ten causes of death worldwide [1-2]. TB primarily affects the lungs (pulmonary TB) with some acute symptoms, but it can also affect other organs (extra-pulmonary TB) of the body [3]. Active tuberculosis symptoms depend on the severity of spread and, generally, include the following clinical features: prolonged cough lasting more than three weeks, blood in the cough (hemoptysis), chest pain, fever, weight loss, and night sweats [4]. Mtb can spread from TB patients to healthy people when patients with TB expel bacteria into the air by coughing or sneezing [5]. According

to the World Health Organization (WHO), in 2019, 10 million TB cases were recorded, with 1.2 million deaths among HIV-negative and 208,000 deaths among HIV-positive [6-7]. The WHO has recommended a standard 6-month administrative treatment for patients suffering from TB. This treatment includes four drugs: isoniazid (INH), rifampicin (RMP), ethambutol (EMB), and pyrazinamide (PZA) [8]. INH is the first-line anti-tubercular compound that is confirmed as an enoyl-acyl carrier protein (ACP) reductase (InhA: EC 1.3.1.9) inhibitor [9]. INH is also known to be a pro-drug requiring activation *via* the Mtb catalase-peroxidase enzyme [10-11]. After activation, INH forms the adduct with nicotine adenine dinucleotide (NADH), which causes the inhibition of InhA, leading to Mtb cell death [12-13]. In the present work, a molecular docking and a 3D-QSAR model study were performed on isoniazid analogues, as potent anti-Mtb agents, to find the structural features important for the

\*Corresponding author. E-mail: [aicha.laoud@gmail.com](mailto:aicha.laoud@gmail.com)

inhibition of the enoyl-ACP reductase enzyme. Then, the results were used to identify new potential enoyl-ACP reductase inhibitors using *in silico* virtual screening. Initially, the ZINC database [14] was filtered by the Lipinski rule of five [15-16] to identify drug-like compounds. The resultant compounds were then docked into the active site of the protein using three different docking parameters (*i.e.*, HTVS, SP, and XP) to re-evaluate their binding ability within the receptor. Finally, the selected hit compounds were submitted to an *in silico* prediction of physicochemical properties to compare the drug-like properties with those of standard medicaments [17].

## MATERIALS AND METHODS

### Dataset and Ligand Preparation

In this study, a dataset of 32 compounds, as potent anti-*Mtb* agents, was collected from the literature [18], and the minimum inhibitory concentration (MIC) values of all ligands were expressed as  $\text{pMIC} = -\log_{10}(\text{MIC})$ , as shown in Table 4. The 3D structure of all ligands was built in Maestro version 9.9.013 (Schrödinger) and prepared by conformational search in MacroModel version 10.3 (Schrödinger) using the OPLS-2005 force field [19]. The conformational search was carried out by applying a mixed torsional/low-mode sampling method [20].

### Molecular Docking

Molecular docking was performed using Glide version 6.2 (Schrödinger) to generate a receptor-based alignment to be then used for developing the 3D-QSAR model. The three-dimensional crystal structure of enoyl-ACP reductase (PDB Id: 2IE0) was extracted from the RCSB PDB website ([www.rcsb.org](http://www.rcsb.org)) with a resolution of 2.20 Å. The protein was prepared using the protein preparation wizard of Schrödinger. Default parameters were used for assigning bond orders, and the OPLS 2005 force field with an average RMSD value of 0.30 Å was used to optimize and minimize the crystal structure [21]. The receptor grid for 2IE0 was generated using receptor grid generation in Maestro [22]. After the generation of the grid, all ligands were docked to the active site of protein using Glide extra-precision (XP) mode [23-24]. The best poses of the ligands were selected based on the Glide XP Score. All ligands were then rescored

to calculate relative binding free energies using the Prime MM-GBSA method [25].

### Development of the 3D-QSAR Model

The 3D-QSAR atom-based model was developed using PHASE version 6.1 (Schrödinger) to explore the relationship between biological activity and different structural features [26]. During model development, all ligands were randomly divided into a training set (75%) and a test set (25%). The atom-based 3D-QSAR model was developed using the 24 molecules of the training set with a grid spacing of 1 Å and a four-partial-least-square (PLS) factor. The best QSAR model was validated by predicting the activities of the 8 test set molecules [27].

### Virtual Screening

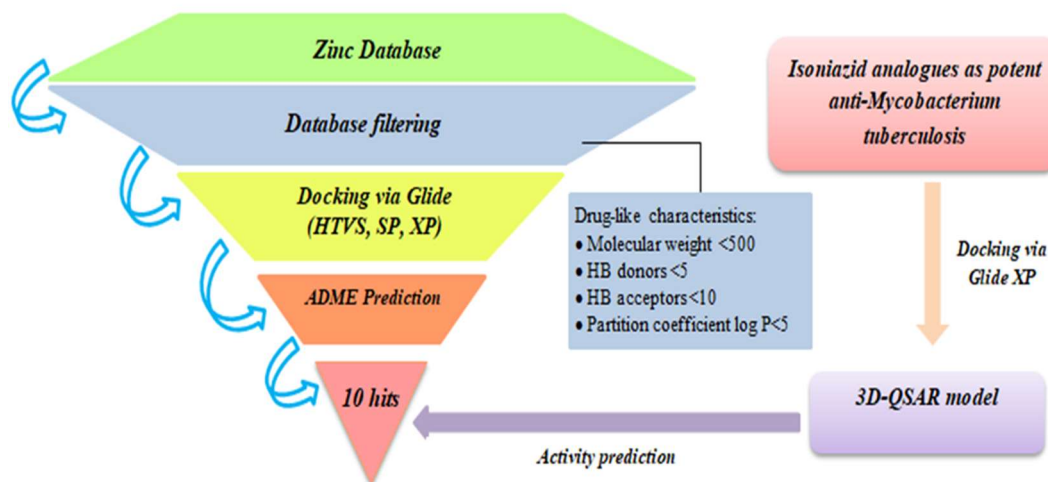
In the present study, the developed model was used to discover new inhibitors of enoyl-ACP reductase against *Mtb* using *in silico* virtual screening.

### Database Filtering

The screening of compounds was performed using the virtual screening workflow in Maestro. Initially, the database was downloaded from an online chemical database called ZINC (<http://zinc15.docking.org/>) and filtered by the Lipinski's Rule of Five (RO5; MW < 500, number of HBD < 5, number of HBA < 10, and partition coefficient (logP) < 5) to identify drug-like molecules [28]. The resulting database was used for the following stages of the study, as depicted in Fig. 1.

### Docking-Based Virtual Screening

The selected compounds were then submitted to molecular docking using three different docking parameters (*i.e.*, HTVS, SP, and XP) [29] to evaluate their binding ability within the active site of the target enzyme. In the first step, the HTVS docking was used, and the top-scoring 10% of docked compounds were selected and subjected to Glide standard precision (SP) docking. Again, 10% of the best-scoring compounds from Glide SP were used for XP docking. Finally, 82 molecules that had an XP-Score > -11.13 were selected for activity prediction and absorption, distribution, metabolism, and excretion (ADME) screening.



**Fig. 1.** The virtual screening workflow for the selected new hit compounds as InhA inhibitors.

### Activity and ADME Prediction

In total, 82 molecules selected from the docking-based virtual screening were subjected to PHASE (Schrodinger) to predict the activity (pMIC) of the hits using the developed 3D-QSAR model (Table 5). Then, the ADME properties of the identified hits were predicted using QikProp version 3.8 (Schrödinger) [30-31] (Table 6).

## RESULTS AND DISCUSSION

### Docking Analysis of Isoniazid Analogues

The analysis of docking into the active site of InhA revealed that isoniazid analogues interacted mainly *via* pi-pi stacking, hydrogen bonds, and hydrophobic interactions. The interactions between ligands 29 and 17 in the enoyl-ACP reductase active site are presented in Fig. 2. The carbonyl group (C=O) of ligands formed hydrogen bond acceptor interactions with ILE194 and THR196 residues. There was a pi-pi stacking interaction between the aromatic ring of the ligand and the amino acid residues PHE149 and TRP222. These interactions were essential for the inhibition of enoyl-ACP reductase. The MM-GBSA rescoring was used to determine the binding energy of the protein-ligand complexes, which provided very high binding free energy. The docking results of the best ligands in the dataset are listed in Table 1.

### 3D-QSAR Model Analysis

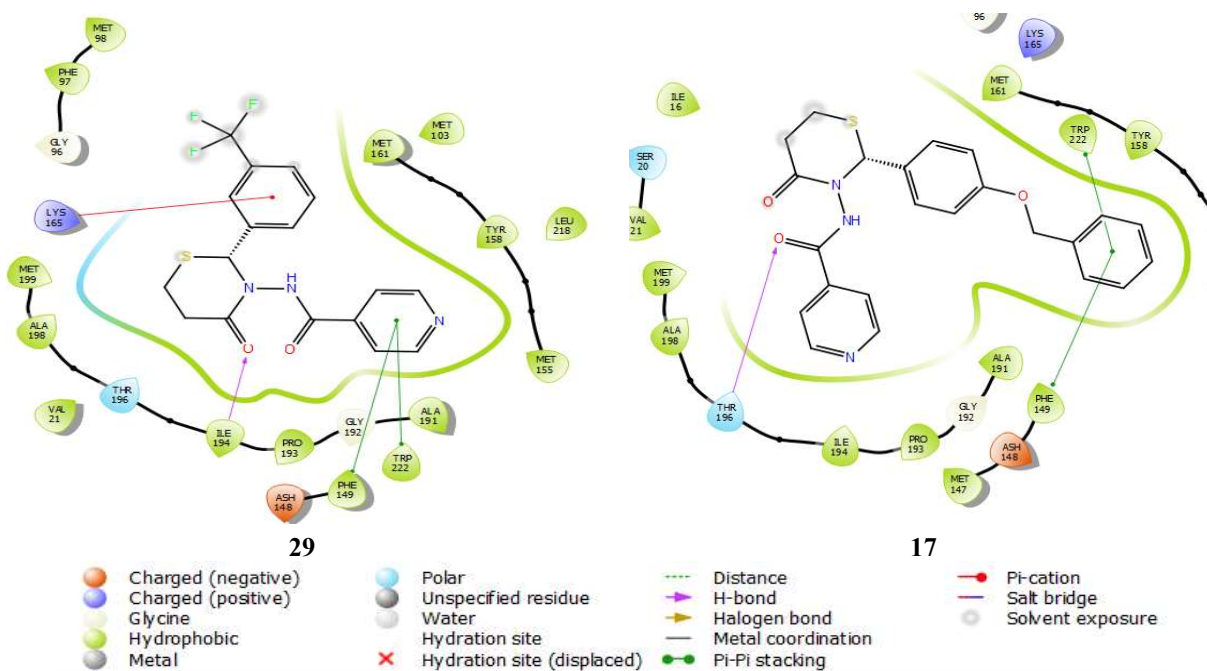
The atom-based 3D-QSAR model was developed

successfully with a four-PLS factor. The developed model had an excellent regression coefficient ( $R^2$ ) of 0.97 for the training set of 24 molecules, a small standard deviation (SD) value of 0.31, a large F value of 178.9, and a stability value of 0.77. Also, the model was validated by a good cross-validation coefficient ( $Q^2$ ) of 0.73 for a test set of 8 molecules with an RMSE of 0.79 and a Pearson ( $r$ ) of 0.86, indicating that the developed model was a robust model with a good predictive ability. Statistical results of the atom-based 3D-QSAR are presented in Table 2.

The correlation between the experimental and predicted activity for the training and test sets is depicted in Fig. 3. The relative contribution of the hydrogen bond donor, hydrophobic group, electron-withdrawing group, and electron-donating group was found to be 4%, 48%, 35%, and 13%, respectively, which indicates the relative importance of hydrophobic and electron-withdrawing groups, as shown in Table 3. The structures and experimental and predicted activity (pMIC) values of the training and test sets are listed in Table 4.

### 3D-QSAR Contour Maps Analysis

The 3D-QSAR visualization provided information that could be used to identify the pharmacophoric properties/features responsible for the inhibition of enoyl-ACP reductase. The contour maps of the model represented 3D characteristics as either blue (favorable regions) or red (unfavorable regions) cubes using the contour visualization module in PHASE [32]. The most active compound (*i.e.*,



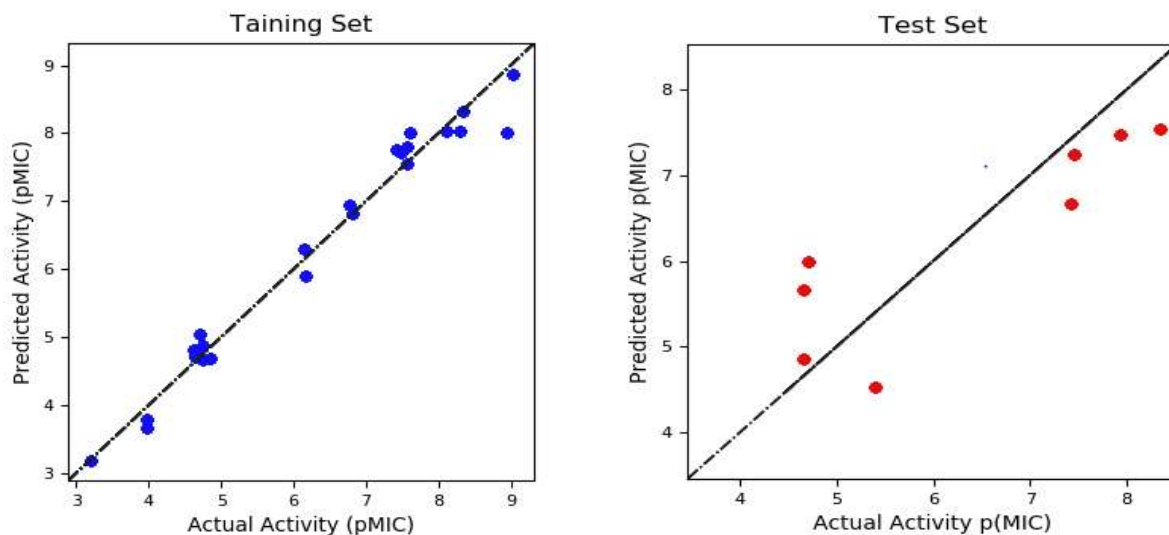
**Fig. 2.** Interaction between ligands 29 and 17 in the enoyl-ACP reductase active site.

**Table 1.** Docking Results of the Best Molecules in the Dataset

Ligands	XP score	Glide E-model	Binding energy	Interacting residues
29	-9.65	-63.95	-64.61	pi-pi = TRP222, PHE149; HBA = ILE194, pi-ca = LYS165
16	-9.46	-78.29	-89.24	pi-pi = TRP222, PHE149
28	-9.31	-66.23	-74.03	pi-pi = TRP222, PHE149; HBA = ILE194
10	-9.26	-65.06	-73.82	pi-pi = TRP222, PHE149; HBA = ILE194
17	-8.97	-73.27	-81.98	pi-pi = TRP222, PHE149, HBA = THR196
2	-8.94	-61.26	-71.71	pi-pi = TRP222, PHE149; HBA = ILE194
26	-8.93	-65.01	-74.16	pi-pi = TRP222, PHE149; HBA = ILE194
23	-8.66	-61.96	-80.39	pi-pi = TRP222, PHE149; HBA = ILE194
18	-8.62	-69.03	-73.26	pi-pi = TRP222, PHE149; HBA = ILE194; pi-ca = LYS165
5	-8.32	-63.59	-81.07	pi-pi = TRP222, PHE149; HBA = ILE194
31	-8.61	-77.96	-89.61	pi-pi = TRP222, PHE149; HBA = LYS165
25	-8.50	-95.90	-67.57	pi-pi = TRP222, PHE149; HBA = ILE194
3	-8.14	-64.86	-72.77	pi-pi = TRP222, PHE149; HBA = ILE194

**Table 2.** PLS Statistics of the Atom-Based 3D-QSAR Model

Factors	SD	R <sup>2</sup>	R <sup>2</sup> <sub>CV</sub>	R <sup>2</sup> <sub>Scramble</sub>	Stability	F	P	RMSE	Q <sup>2</sup>	Pearson (r)
1	1.37	0.42	0.06	0.33	0.85	16.2	0.00057	0.99	0.57	0.81
2	0.64	0.88	0.47	0.62	0.65	76.7	2.21e-10	0.80	0.72	0.87
3	0.46	0.94	0.64	0.80	0.75	104.6	2.14e-12	0.79	0.72	0.87
4	0.31	0.97	0.71	0.92	0.77	178.9	8.53e-15	0.79	0.73	0.86



**Fig. 3.** The correlation between the experimental and predicted activity (pMIC) of the training and test set molecules.

**Table 3.** The Values Calculated for the Four-PLS Factor for the 3D-QSAR Model

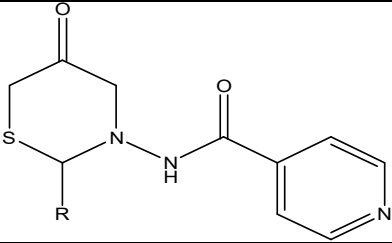
Factors	H-bond donor	Hydrophobic group	Negative ionic	Positive ionic	Electron-withdrawing	Electron-donating
1	0.02	0.54	0.00	0.00	0.30	0.13
2	0.03	0.46	0.00	0.00	0.35	0.15
3	0.03	0.48	0.00	0.00	0.34	0.14
4	0.04	0.48	0.00	0.00	0.35	0.13

compound 29) (MIC = 0.52  $\mu$ M) was selected as the reference compound for the visualization of contour maps (Fig. 4). The hydrogen bond donor interaction showed only blue cubes near the NH group of the ligands. The hydrophobic interaction showed blue cubes near the fluorophenyl groups of the ligands. Moreover, blue cubes were observed across the entire aromatic ring of the ligands. The electron-withdrawing group showed blue cubes near the carbonyl groups (C=O) of the ligands. As regards the electron-donating group, while blue cubes were favored for inhibitory activity against the enoyl-ACP reductase, red cubes were not considered for the activity prediction.

### Docking Analysis of Hits

Molecular Docking into the active site residues of InhA revealed that virtual screening hits can interact analogously with isoniazid analogues. The analysis of the docking

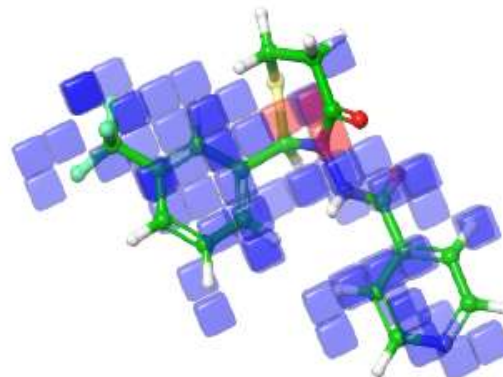
interaction of virtual screening hits (Fig. 5) showed that the majority of the pi-pi stacking interactions occurred in PHE149 and TRP222 amine acid residues via an aromatic ring group of hits. While the hydrogen bond acceptor interactions were observed in the THR196 and ILE194 residues *via* a carbonyl group (C=O) of hits, the hydrogen bond donor interaction was observed in the GLY192 residue *via* an NH group of hits. The XP Glide score of the identified hits (ranging from -11.13 to -13.41 kcal mol<sup>-1</sup>) was better than the XP Glide score of the isoniazid analogues (range: -6.18. to -9.65 kcal mol<sup>-1</sup>), suggesting that the identified hits had a higher binding affinity for the inhibition of InhA. The interactions of the final 10 hits in the active site of enoyl-ACP reductase are presented in Fig. 5. The docking results of these final 10 hits with their predicted activity (pMIC) are listed in Table 5.

**Table 4.** Structures, Experimental *Versus* Predicted Activity, and the Residuals of the Training and Test Sets\*


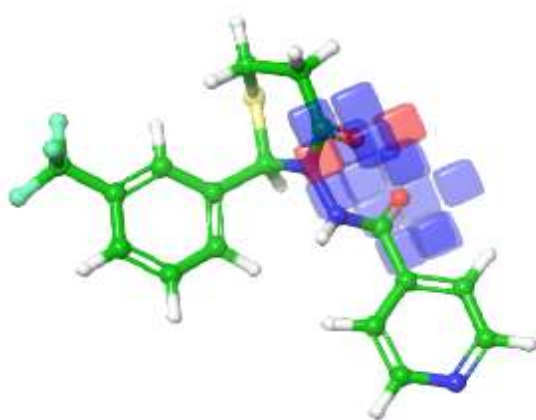
Compounds	R	Experimental pMIC	PLS	Predicted pMIC	Residual
1	Ph	4.62	4	4.81	0.19
2*	Ph-(2-Me)	4.65	4	4.86	0.21
3	Ph-(3-Me)	4.65	4	4.70	0.05
4	Ph-(4-Me)	4.65	4	4.75	0.10
5*	Ph-(2-OMe)	4.70	4	5.99	1.29
6	Ph-(3-OMe)	4.70	4	5.05	0.35
7*	Ph-(4-OMe)	5.39	4	4.52	-0.87
8	Ph-(3,4,5-OMe)	4.86	4	4.68	-0.18
9	Ph-(3-OH, 4-OMe)	4.75	4	4.68	-0.07
10	Ph-(2-OH)	3.97	4	3.79	-0.18
11*	Ph-(3-OH)	4.66	4	5.67	1.01
12	Ph-(4-OH)	3.97	4	3.66	-0.31
13	Ph-(3-N(Me) <sub>2</sub> )	4.73	4	4.88	0.15
14	Ph-(4-(CH(Me) <sub>2</sub> ))	6.15	4	6.30	0.15
15*	Ph-(2-OCH <sub>2</sub> Ph)	8.33	4	7.54	-0.79
16	Ph-(3-OCH <sub>2</sub> Ph)	8.33	4	8.32	-0.01
17	Ph-(4-OCH <sub>2</sub> Ph)	9.03	4	8.87	-0.16
18	Ph-(2-NO <sub>2</sub> )	6.16	4	5.91	-0.25
19	Ph-(3-NO <sub>2</sub> )	7.49	4	7.72	0.23
20	Ph-(4-NO <sub>2</sub> )	6.80	4	6.82	0.02
21	Ph-(2-Cl)	6.77	4	6.95	0.18
22*	Ph-(4-Cl)	7.46	4	7.24	-0.22
23	Ph-(2-Br)	8.29	4	8.04	-0.25
24	Ph-(4-Br)	7.60	4	8.01	0.41
25	Ph-(2-F)	7.42	4	7.77	0.35
26*	Ph-(3-F)	7.42	4	6.66	-0.76
27	Ph-(4-F)	8.11	4	8.03	-0.08
28	Ph-(2-CF <sub>3</sub> )	7.56	4	7.55	-0.01
29	Ph-(3-CF <sub>3</sub> )	7.56	4	7.81	0.25
30	Ph-(4-CF <sub>3</sub> )	8.95	4	8.00	-0.95
31	2-Furfuryl	3.19	4	3.18	-0.01
32*	2-Furfuryl-(5-NO <sub>2</sub> )	7.93	4	7.47	-0.46



Visualization of the hydrogen bond donor effect



Visualization of the hydrophobic effect



Visualization of the electron-withdrawing effect



Visualization of the electron-donating effect

**Fig. 4.** QSAR visualization for the most active compound (*i.e.*, compound 29).

### ADME Prediction of Hits

The ADME properties (Table 6) of the 10 hits were found to be within the acceptable range intended for human use, which renders them potential drug-like compounds.

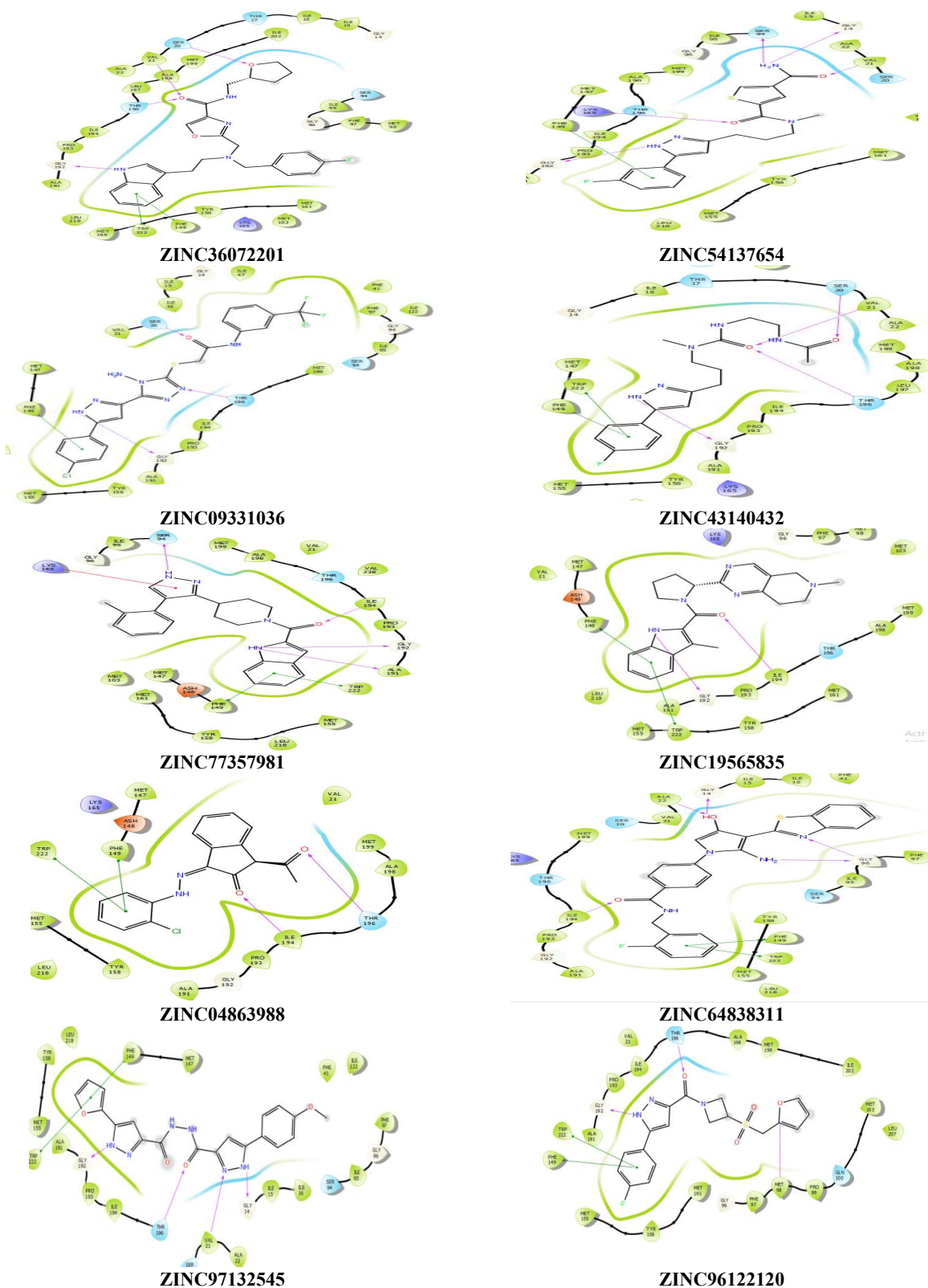
### CONCLUSIONS

Two computational approaches were applied to investigate the relationship between the structure, activity, and interaction mechanism of the isoniazid analogues on the active site of InhA. The atom-based 3D-QSAR developed model resulted in acceptable statistics ( $R^2 = 0.97$  of the training set,  $Q^2 = 0.73$  of the test set). The docking results showed that TRP222, PHE149, LYS194, and THR196 were

important amino acids in the receptor active site to interact with the ligands. In parallel, 10 hits were identified as potent anti-Mtb with their predicted activity determined using *in silico* virtual screening approach. The results of this work may provide valuable clues for the discovery of new enoyl-ACP reductase inhibitors of Mtb.

### ACKNOWLEDGEMENTS

The authors would like to gratefully acknowledge the financial help provided by the Directorate General for Scientific Research and Technological Development (DGRSDT), Algeria.



**Fig. 5.** Interactions of the final 10 selected hits in the active site of InhA.



**Table 5.** The Docking Results of the 10 Hits with Their Predicted Activity (pMIC)

Hits	Interacting residues	XP Score	Glide E-model	Binding energy	P(MIC)
ZINC36072201	pi-pi = TRP222, PHE149; HBA = THR196, VAL21, SER20; HBD = GLY192	-13.41	-98.48	-71.47	5.53
ZINC54137654	pi-pi = PHE149; HBA = LYS165, VAL21 HBD = GLY192, SER94, GLY14	-12.94	-93.24	-76.21	6.46
ZINC09331036	pi-pi = PHE149; HBA = THR196, SER 20 HBD = GLY192	-12.75	-98.07	-81.60	6.58
ZINC43140432	pi-pi = PHE149, TRP222; HBA = THR 196, VAL21, SER20; HBD = GLY192	-12.50	-91.69	-81.87	6.87
ZINC77357981	pi-pi = PHE149, TRP222; $\pi$ -Cation = LYS165; HBA = ILE194; HBD = GLY192, SER94, ALA191	-12.37	-77.18	-56.39	7.32
ZINC19565835	pi-pi = PHE149, TRP222; HBA = ILE194 HBD = GLY192	-12.03	-68.15	-57.74	6.72
ZINC04863988	pi-pi = PHE149, TRP222; HBA = THR196, ILE194	-11.99	-57.43	-62.74	6.43
ZINC64838311	pi-pi = PHE149, TRP222; HBA = ILE194, ALA22, GLY96; HBD = GLY96, GLY14	-11.69	-88.13	-62.13	6.37
ZINC97132545	pi-pi = PHE149, TRP222; HBA = THR 196, VAL21; HBD = GLY192, GLY14	-11.54	-102.93	-79.44	6.33
ZINC96122120	pi-pi = PHE149, TRP222; HBA = THR196; HBD = GLY192	-12.52	-82.03	-68.03	6.64

**Table 6.** ADME Properties of the 10 Hits and the most Active Compound (*i.e.*, Compound 29) in the Dataset

Hits	MW <sup>a</sup>	dHB <sup>b</sup>	aHB <sup>c</sup>	QPlogPw <sup>d</sup>	QPlogP0/w <sup>e</sup>	QPlogS <sup>f</sup>	QPPCaco <sup>g</sup>	PHOA <sup>h</sup>	HOA <sup>i</sup>
ZINC36072201	476.55	2	8.2	13.97	4.61	-5.81	299.29	100	3
ZINC54137654	386.44	3	6.5	13.98	2.83	-5.36	134.94	81.66	3
ZINC09331036	493.89	4	7.5	17.39	3.54	-6.38	45.74	77.38	1
ZINC43140432	361.42	3	5.5	16.34	2.47	-4.59	122.98	78.80	3
ZINC77357981	384.48	2	4.5	11.99	4.63	-6.68	1003.67	100	1
ZINC64838311	458.51	4	5.25	16.09	4.99	-7.36	578.81	100	1
ZINC04863988	312.76	0.5	5	6.32	3.24	-2.85	2196.29	100	3
ZINC19565835	375.47	1	7	11.38	3.19	-4.44	530.71	94.40	3
ZINC97132545	392.37	0.5	4.75	10.11	3.63	-6.69	62.88	80.41	1
ZINC96122120	389.40	0	6.5	9.90	3.10	-4.53	425.21	92.17	3
29	381.37	0.25	6.25	9.48	3.44	-4.63	1361.31	100	3
Rule	< 500	0-6	2- 20	4 - 45	-2.0 - 6.5	-6.5 - 0.5	< 25 poor > 500 great	> 80% high < 25% low	1 low 3 high

<sup>a</sup>Molecular weight. <sup>b</sup>Hydrogen bond donors. <sup>c</sup>Hydrogen bond acceptors. <sup>d</sup>Predicted water/gas partition coefficient. <sup>e</sup>Predicted octanol/water partition coefficient. <sup>f</sup>Predicted aqueous solubility, logarithm in mol dm<sup>-3</sup>. <sup>g</sup>Predicted apparent Caco-2 cell permeability in nm s<sup>-1</sup>. <sup>h</sup>Percent human oral absorption. <sup>i</sup>Human oral absorption.

## REFERENCES

- [1] Deshmukh, T. R.; Khare, S. P.; Krishna, V. S.; *et al.*, Synthesis, bioevaluation and molecular docking study of new piperazine and amide linked dimeric 1,2,3-triazoles. *Synth. Commun.*, **2020**, *50*, 271-288, DOI: 10.1080/00397911.2019.1695275.
- [2] Shola Adeniji, E.; Uba, S.; Uzairu, A., A novel QSAR model for the evaluation and prediction of (E)-N'-benzylideneisonicotinohydrazide derivatives as the potent anti-mycobacterium tuberculosis antibodies using genetic function approach. *Phys. Chem. Res.*, **2018**, *6*, 479-492, DOI: 10.22036/pcr.2018.115878.1457.
- [3] Joshi, S. D.; More, U. A.; Dixit, S. R.; *et al.*, Chemical synthesis and *in silico* molecular modeling of novel pyrrolyl benzohydrazide derivatives: Their biological evaluation against enoyl ACP reductase (InhA) and Mycobacterium tuberculosis. *Bioorg. Chem.*, **2017**, *75*, 181-200, DOI: 10.1016/j.bioorg.2017.09.008.
- [4] KumarHalderab, S.; Elmaa, F., *In silico* identification of novel chemical compounds with anti-TB potential for the inhibition of InhA and EthR from Mycobacterium tuberculosis. *J. Clin. Tuberc. Other. Mycobact. Dis.*, **2021**, *24*, 1-9, DOI: 10.1016/j.jctube.2021.100246.
- [5] Prasasty, V. D.; Cindana, S.; Ivan, F. X.; *et al.*, Structure-based discovery of novel inhibitors of Mycobacterium tuberculosis CYP121 from Indonesian natural products. *Comput. Biol. Chem.*, **2020**, *85*, 107205, DOI: 10.1016/j.compbiolchem.2020.107205.
- [6] Chakaya, J.; Khan, M.; Ntoumi, F.; *et al.*, Global Tuberculosis Report 2020-Reflections on the Global TB burden, treatment and prevention efforts. *Int. J. Infect. Dis.*, **2021**, *113*, S7-S12, DOI: 10.1016/j.ijid.2021.02.107.
- [7] Phanumartwiwath, A.; Kesornpun, C.; Sureram, S.; *et al.*, Antitubercular and antibacterial activities of isoxazolines derived from natural products: Isoxazolines as inhibitors of Mycobacterium tuberculosis InhA. *J. Chem. Res.*, **2021**, *45*, 1003-1015, DOI: 10.1177/17475198211047801.
- [8] Nayak, N.; Ramprasad, J.; Dalimba, U., New INH-pyrazole analogs: Design, synthesis and evaluation of antitubercular and antibacterial activity. *Bioorg. Med. Chem. Lett.*, **2015**, *25*, 5540-5545, DOI: 10.1016/j.bmcl.2015.10.057.
- [9] Khade, A. B.; Eshwara, V. K.; Boshoff, H. I. M.; *et al.*, Design, synthesis, biological evaluation and Molecular dynamic simulation studies of diphenyl ether derivatives as antitubercular and antibacterial agents. *Struct. Chem.*, **2020**, *31*, 983-998, DOI: 10.1007/s11224-019-01478-8.
- [10] Rawat, R.; Whitty, A.; Tonge, P. J., The isoniazid-NAD adduct is a slow, tight-binding inhibitor of InhA, the Mycobacterium tuberculosis enoyl reductase: Adduct affinity and drug resistance. *Proc. Natl. Acad. Sci.*, **2003**, *100*, 13881-13886, DOI: 10.1073/pnas.2235848100.
- [11] Holas, O.; Ondrejcek, P.; Dolezal, M., Mycobacterium tuberculosis enoyl-acyl carrier protein reductase inhibitors as potential antitubercotics: Development in the past decade. *J. Enzyme Inhib. Med. Chem.*, **2015**, *30*, 629-648, DOI: 10.3109/14756366.2014.959512.
- [12] Chollet, A.; Mourey, L.; Lherbet, C.; *et al.*, Crystal structure of the enoyl-ACP reductase of Mycobacterium tuberculosis (InhA) in the apo-form and in complex with the active metabolite of isoniazid pre-formed by a biomimetic approach. *J. Struct. Biol.*, **2015**, *190*, 328-337, DOI: 10.1016/j.jsb.2015.04.008.
- [13] Shahbaaz, M.; Qari, S. H.; Abdellattif, M. H.; Hussien, M. A., Structural analyses and classification of novel isoniazid resistance coupled mutational landscapes in Mycobacterium tuberculosis: a combined molecular docking and MD simulation study. *J. Biomol. Struct. Dyn.*, **2020**, *0*, 1-10. DOI: 10.1080/07391102.2020.1861986.
- [14] Irwin, J. J.; Shoichet, B. K., ZINC-A free database of commercially available compounds for virtual screening, *J. Chem. Inf. Model*, **2005**, *45*, 177-182, DOI: 10.1021/ci049714+.
- [15] Lipinski, C. A., Drug-like properties and the causes of poor solubility and poor permeability. *J. Pharmacol. Toxicol. Methods*, **2000**, *44*, 235-249, DOI: 10.1016/S1056-8719(00)00107-6.
- [16] Lipinski, C. A.; Lombardo, F.; Dominy, B. W., Feeney, P. J., Experimental and computational approaches to estimate solubility and permeability in drug discovery

- and developmental settings. *Adv. Drug Deliv. Rev.*, **1997**, *23*, 3-25, DOI: 10.1016/S0169-409X(96)00423-1.
- [17] Kulkarni, V. M.; Bhansali, S., Pharmacophore generation, atom-based 3D-QSAR, docking, and virtual screening studies of p38- $\alpha$ ; mitogen activated protein kinase inhibitors: pyridopyridazin-6-ones (part 2). *Res. Reports Med. Chem.*, **2013**, *4*, 1-21, DOI: 10.2147/rrmc.s50738.
- [18] Ramani, A. V.; Monika, A.; Indira, V. L.; *et al.*, Synthesis of highly potent novel anti-tubercular isoniazid analogues with preliminary pharmacokinetic evaluation. *Bioorg. Med. Chem. Lett.*, **2012**, *22*, 2764-2767. DOI: 10.1016/j.bmcl.2012.02.091.
- [19] Jorgensen, W. L.; Tirado-Rives, J., The OPLS potential functions for proteins. Energy minimizations for crystals of cyclic peptides and crambin. *J. Am. Chem. Soc.*, **1988**, *110*, 1657-66, DOI: 10.1021/ja00214a001.
- [20] Laoud, A.; Ferkous, F.; Maccari, L.; *et al.*, Identification of novel nt-MGAM inhibitors for potential treatment of type 2 diabetes: Virtual screening, atom based 3D-QSAR model, docking analysis and ADME study. *Comput. Biol. Chem.*, **2018**, *72*, 122-135, DOI: 10.1016/j.compbiolchem.2017.12.003.
- [21] Sharma, R.; Kothapalli, R.; van Dongen, A. M. J.; Swaminathan, K., Chemoinformatic identification of novel inhibitors against Mycobacterium tuberculosis l-aspartate  $\alpha$ -decarboxylase. *PLoS One*, **2012**, *7*, e33521, DOI: 10.1371/journal.pone.0033521.
- [22] Lobo, M. J.; Ray, R.; Shenoy, G. G., Gaining deeper insights into the surface binding of bedaquiline analogues with the ATP synthase subunit C of: Mycobacterium tuberculosis using molecular docking, molecular dynamics simulation and 3D-QSAR techniques. *New J. Chem.*, **2020**, *44*, 18831-18852, DOI: 10.1039/d0nj02062a.
- [23] Zaccagnini, L.; Brogi, S.; Brindisi, M.; *et al.*, Identification of novel fluorescent probes preventing PrPSc replication in prion diseases, *Eur. J. Med. Chem.*, **2017**, *127*, 859-873, DOI: 10.1016/j.ejmech.2016.10.064.
- [24] Friesner, R. A.; Murphy, R. B.; Repasky, MP.; *et al.*, Extra precision glide: Docking and scoring incorporating a model of hydrophobic enclosure for protein-ligand complexes, *J. Med. Chem.*, **2006**, *49*, 6177-6196, DOI: 10.1021/jm051256o.
- [25] Fan, N.; Zhang, S.; Sheng, T.; *et al.*, Docking field-based QSAR and pharmacophore studies on the substituted pyrimidine derivatives targeting HIV-1 reverse transcriptase. *Chem. Biol. Drug. Des.*, **2018**, *91*, 398-407, DOI:10.1111/cbdd.13086.
- [26] Panwar, U.; Singh, SK., Atom-based 3D-QSAR, molecular docking, DFT, and simulation studies of acylhydrazone, hydrazine, and diazene derivatives as IN-LEDGF/p75 inhibitors. *Struct. Chem.*, **2021**, *32*, 337-352, DOI: 10.1007/s11224-020-01628-3.
- [27] Chedadia, O.; El Aissouq, A.; El Ouardic, Y.; *et al.*, *In silico* prediction of novel (TRIM24) bromodomain Inhibitors: A combination of 3D-QSAR, molecular docking, ADMET prediction, and molecular dynamics. *Phys. Chem. Res.*, **2022**, *10*, 519-535, DOI: 10.22036/PCR.2022.331866.2040.
- [28] El McHichi, L.; El Aissouq, A.; Kasmi, R.; *et al.*, *In silico* design of novel Pyrazole derivatives containing thiourea skeleton as anti-cancer agents using: 3D QSAR, Drug-Likeness studies, ADMET prediction and molecular docking. *Mater. Today Proc.*, **2021**, *45*, 7661-7674, DOI: 10.1016/j.matpr.2021.03.152.
- [29] Madhavaram, M.; Nampally, V.; Gangadhari, S.; *et al.*, High-throughput virtual screening, ADME analysis, and estimation of MM/GBSA binding-free energies of azoles as potential inhibitors of Mycobacterium tuberculosis H37Rv. *J. Recept Signal Transduct*, **2019**, *39*, 312-320, DOI: 10.1080/10799893.2019.1660895.
- [30] Elmchichi, L.; Belhassan, A.; Lakhlifi, T.; Bouachrine M., 3D-QSAR study of the chalcone derivatives as anticancer agents. *J. Chem.*, **2020**, 1-12, DOI: 10.1155/2020/5268985.
- [31] Wang, Y.; Xing, J.; Xu, Y.; *et al.*, *In silico* ADME/T modelling for rational drug design. *Q Rev. Biophys.*, **2015**, *48*, 488-515, DOI: 10.1017/S0033583515000190.
- [32] Mishra, N.; Maurya, A. K.; Mulpuru, V., Discovery of novel coumarin analogs against the  $\alpha$ -glucosidase protein target of diabetes mellitus: Pharmacophore-based QSAR, docking, and molecular dynamics simulation studies. *ACS Omega*. **2020**, *5*, 32234-32249, DOI: 10.1021/acsomega.0c03871.